RSC Advances

PAPER

View Article Online
View Journal | View Issue

Cite this: *RSC Adv.*, 2014, **4**, 22743

A 4-*tert*-butylcalix[4]arene tetrahydroxamate podand based on the 1-oxypiperidine-2-one (1,2-PIPO$^-$) chelate. Self-assembly into a supramolecular ionophore driven by coordination of tetravalent zirconium or hafnium(IV)†

Pawel Jewula, Jean-Claude Chambron,* Marie-José Penouilh, Yoann Rousselin and Michel Meyer*

Received 4th February 2014
Accepted 30th April 2014

DOI: 10.1039/c4ra00977k

www.rsc.org/advances

An octadentate tetrahydroxamic calix[4]arene podand incorporating 1-hydroxypiperidine-2-one (1,2-PIPOH) binding units has been designed as a specific chelator for tetravalent metal cations like Zr^{4+} or Hf^{4+}. This receptor, which can be considered as the first ever abiotic ligand possessing only cyclic six-membered hydroxamate groups, has been synthesized and characterized in its tetraprotonated form ($\mathbf{1}H_4$). Contrary to expectation, however, this new chelator did not form a 1 : 1 complex upon reaction with $M(acac)_4$ (M = Zr and Hf; acac = acetylacetonate), but rather self-assembled into a dimeric species of 2 : 2 stoichiometry. The latter could be characterized in solution by mass spectrometry and NMR spectroscopy as its monopotassium adduct ($[M_2K(\mathbf{1})_2]^+$), pointing to the ionophoric character of the $M_2(\mathbf{1})_2$ complex.

Introduction

Zirconium(IV) is a d^0 hard tetravalent transition metal cation and a great variety of its open-sphere complexes have been developed as Lewis acid polymerization catalysts over the past decades.[1] By contrast, a field of research where the coordination chemistry of Zr^{4+} has been recently involved is molecular imaging.[2] Indeed, the ^{89}Zr isotope has been identified as very promising for the engineering of antibody-based radiotracers for positron emission tomography (PET) imaging, because its half-life of 78.4 h (~3 days) is commensurable with the biodistribution half-life of IgG antibodies (a few days), which is not the case of ^{64}Cu and ^{86}Y, the latter being also more expensive to produce. However as it is, non-osteophilic chelation systems are required that encapsulate the radioactive cation and prevent it from being uptaken into bone tissues. With few exceptions, $^{89}Zr^{4+}$-based radiopharmaceuticals under development incorporate desferrioxamine B (DFO) as chelator,[2] because of the high affinity of hydroxamates for zirconium(IV)[3] and the ready availability and non-toxicity of this industrially-produced siderophore. In addition, the pendant amine function has been used to advantage for bioconjugation.[2f] However, DFO is a hexadentate chelator that cannot fully satisfy the typical coordination number of Zr^{4+} (*i.e.* CN = 8), and the use of oxygen-rich octadentate ligands (for example catecholates, hydroxypyridonates, or hydroxamates) has been suggested recently.[2f] In this respect, the now commercially available 3,4,3-LI(1,2-HOPO) ligand, based on 1,2-hydroxypyridinone (1,2-HOPO), could represent a possible alternative to DFO. Indeed, the complex of 1,2-HOPO$^-$ with Zr^{4+} has been synthesized and characterized,[4] while $[3,4,3\text{-LI}(1,2\text{-HOPO})]^{3-}$ forms extraordinarily stable complexes with tetravalent Ce^{4+} ($\log \beta_{110} = 41.5$), and Th^{4+} ($\log \beta_{110} = 40.1$),[5] and it is currently considered as one of the most promising *in vivo* decorporation agent for actinides.[6]

We have recently undertaken a research program aimed at exploring the coordination properties of 1-hydroxypiperidine-2-one (1,2-PIPOH, Fig. 1), a six-membered cyclic hydroxamic acid

1,2-HOPO 1,2-PIPOH

Fig. 1 Structural formulae of 1,2-HOPO and 1,2-PIPOH.

Institut de Chimie Moléculaire de l'Université de Bourgogne (ICMUB), UMR CNRS 6302, 9 avenue A. Savary, BP 47870, 21078 Dijon Cedex, France. E-mail: jean-claude.chambron@u-bourgogne.fr; michel.meyer@u-bourgogne.fr; Fax: +33 3 80 39 61 17; Tel: +33 3 80 39 61 16

† Electronic supplementary information (ESI) available: Tables of crystallographic data for $\mathbf{1}Bn_4$; copies of the mass and NMR spectra of $\mathbf{1}Bn_4$ and $\mathbf{1}H_4$ (including 2D correlation maps); copies of the ^{1}H NMR spectra of $[Na(\mathbf{1}H_4)]Cl$ and $[K(\mathbf{1}H_4)]Cl$; copies of the ^{1}H NMR spectra of $Zr_2(\mathbf{1})_2$ and $Hf_2(\mathbf{1})_2$; copies of the mass and NMR spectra of $[Hf_2K(\mathbf{1})_2]Cl$ (including 2D correlation maps) and $[Zr_2K(\mathbf{1})_2]Cl$ (^{1}H NMR spectrum). CCDC 983068. For ESI and crystallographic data in CIF or other electronic format see DOI: 10.1039/c4ra00977k

that is found as third, pendent binding unit in a few number of siderophores such as exochelin MN[7] and tsukubachelin.[8] Structural studies revealed as expected the formation of tetraleptic complexes with tetravalent d- and f-block elements, including Zr^{4+}, Ce^{4+}, Hf^{4+}, Th^{4+}, and U^{4+}.[3g] As the binding sites of 1,2-PIPO$^-$ are incorporated in a cyclic structure similarly to 1,2-HOPO$^-$, the former is also a ligand preorganized for chelation, therefore its complexes should be more stable than those originating from linear hydroxamates which prevail in solution in their *E* or *trans* form. In exochelin MN and other related siderophores, an amide nitrogen atom attached at the *R*-stereogenic, C-3 carbon atom of the 1,2-PIPOH moiety connects it to the main chain of the molecule.[9] With the natural design in mind, we decided to synthesize a tetrachelating podand by grafting four 1,2-PIPOH residues to the calix[4]arene platform for the efficient sequestration of octacoordinated tetravalent cations such as Zr^{4+}. We chose calix[4]arene as an alternative to the open-chain or branched polyamine-type backbones in order to impart a C_4-symmetric propeller-like arrangement of the chelating units around the metal centre expected to adopt a square-antiprismatic coordination geometry (Fig. 2). Moreover, the large rim can, in principle, be easily functionalized by water-solubilising groups.[10]

In fact, calixarenes have been widely used as a platform for constructing a variety of podands including hydroxamate chelators,[11] but tetrahydroxamates based on calix[4]arene are very scarce.[12] For example, Gopalan and coworkers reported in 1997 the design, synthesis, and use for thorium(IV) extraction of 4-*tert*-butylcalix[4]arenes carrying the simplest linear hydroxamate ligands connected from the carbonyl side to the oxygen atoms of the lower rim through a *n*-butyl chain.[12c] Inspired by this work, we designed the podand $\mathbf{1}H_4$ in which the same number of atoms (4) separates the phenolic oxygen and the carbonyl carbon atoms of the 1,2-PIPOH chelating units.

This report describes the synthesis and solution characterisation of the tetrapod $\mathbf{1}H_4$, together with a detailed spectroscopic (NMR and HR-MS) study of the reaction products obtained with zirconium(IV) and hafnium(IV). We show that instead of forming the expected 1 : 1 complexes (Fig. 2), receptor **1** affords binuclear 2 : 2 species which can moreover take up an additional alkali-metal cation, thus acting as an ionophore. These results will be interpreted and rationalized in light of the structural features exhibited by the Zr(1,2-PIPO)$_4$ and Hf(1,2-PIPO)$_4$ complexes.[3g]

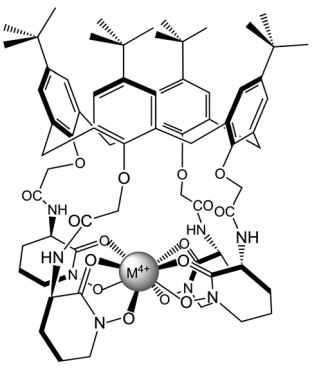

Fig. 2 The anticipated complex of podand $\mathbf{1}H_4$ with tetravalent metal cations Zr^{4+} and Hf^{4+}.

Results and discussion

Ligand design and synthesis

The direct precursors of $\mathbf{1}H_4$ (Scheme 1) are the hydrobromide salt of (*R*)-3-amino-1-benzyloxypiperidin-2-one (**7**)[13] and the acetyl chloride derivative of *p-tert*-butylcalix[4]arene (**8**)[12b,14] (Scheme 2). The former was synthesized in four steps and 19% overall yield from commercially available Cbz-protected L-ornithine **2**, according to the reaction sequence shown in Scheme 1.[13,15] At first, this reagent was condensed with benzaldehyde in basic conditions to afford imine **3**,[15] which was subsequently oxidized with *m*-CPBA to oxaziridine **4**. The latter was reacted with trifluoroacetic acid in dichloromethane, which allowed us to isolate the nitrone **5** in 42% overall yield after purification by crystallization. Next, **5** was reacted with hydroxylamine to form the desired cyclic hydroxamic acid,[13] which was not isolated but immediately protected by reaction with benzylbromide to afford the synthon **6**. The amino group was selectively deprotected by 33% HBr in acetic acid to give the hydrobromide salt (*R*)-**7**·HBr in 90% yield. Subsequently, the benzyl-protected tetrapod $\mathbf{1}Bn_4$ was prepared by coupling the acid chloride derivative **8** with four equivalents of **7**·HBr in the presence of triethylamine (Scheme 2). The modified calix[4]arene $\mathbf{1}Bn_4$ was obtained in 50% isolated yield by fractional crystallization from methanol.‡ Deprotection of $\mathbf{1}Bn_4$ to $\mathbf{1}H_4$ was accomplished by hydrogenolysis in methanol at room temperature using 20% Pd(OH)$_2$/C as catalyst. Smooth conditions were used as 10% Pd/C catalyses the cleavage of benzyl carbamates by dihydrogen.[16] However, even in these mild conditions, the reaction time (15 min) was a critical parameter. Indeed, as shown by MALDI-TOF mass spectrometry analysis, longer periods resulted in the hydrogenolysis of the hydroxamic acid N–O bonds. By applying the optimal conditions, the tetrahydroxamic acid $\mathbf{1}H_4$ was isolated in 93% yield after filtration on a short pad of silica gel.

X-ray crystal structure analysis of $\mathbf{1}Bn_4$

Slow evaporation of a methanolic solution of the benzyl-protected receptor afforded X-ray quality crystals of $\mathbf{1}Bn_4 \cdot 0.75CH_3OH \cdot 0.25H_2O$ composition. An ORTEP view[17] of the molecular structure of $\mathbf{1}Bn_4$ is shown in Fig. 3, together with the atom labelling scheme. The calix[4]arene platform adopts a pinched-cone conformation in the solid state as found in the structure of numerous other related compounds that carry substituents at the lower rim in order to prevent ring flipping.[18] The angles that the four aromatic rings (A–D) make with the

‡ We observed that attempts to purify crude $\mathbf{1}Bn_4$ by flash column chromatography (35–70 μm silica gel) led to a product featuring the same MALDI-TOF mass spectrum as the one of the $\mathbf{1}Bn_4$ samples isolated by crystallization and characterized unambiguously by X-ray crystallography. However, its ^{1}H and ^{13}C NMR spectra differed from the ones corresponding to $\mathbf{1}Bn_4$, pointing to some unexplained isomerization or conformational change.

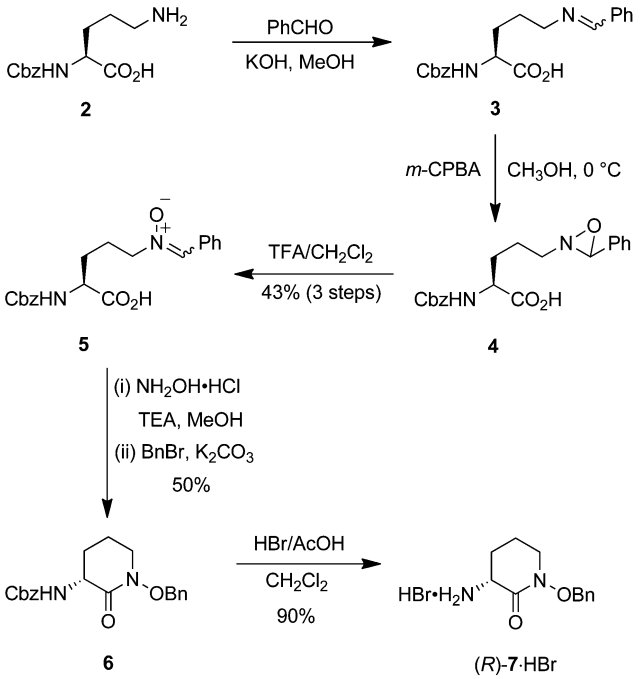

Scheme 1 Synthesis of 7·HBr from Cbz-protected L-ornithine 2.[13,15]

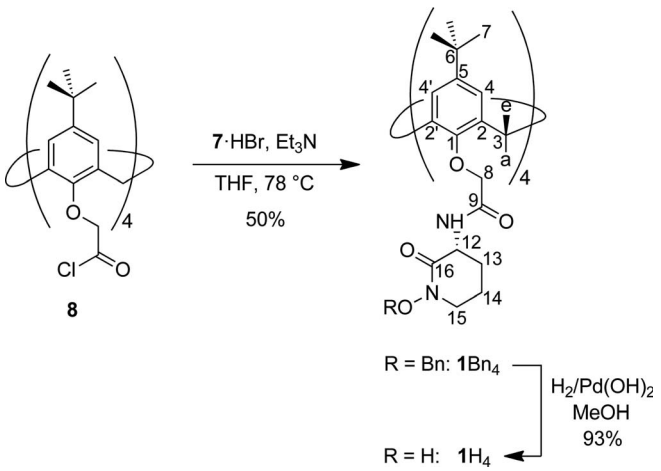

Scheme 2 Functionalization of calix[4]arene with the 1,2-PIPOH chelate. The C-atom numbering scheme used in the NMR data assignment is also shown.

mean plane of the four bridging methylene groups (C1, C12, C23, and C34) are 36.6(1) (A), 87.0(1) (B), 47.6(9) (C), and 84.8(1)° (D), respectively. Therefore, rings A and C are strongly tilted, being practically normal to each other [interplanar angle of 84.2(1)°], while rings B and D are approximately parallel to each other [interplanar angle of 2.7(2)°]. The electron lone pairs of the four phenolic oxygen atoms O1, O2, O3, and O4 are all pointing towards the cavity interior. Each piperidine-2-one ring was shown to adopt a half-chair conformation by ring puckering analysis (Table S6, ESI†),[19] and to exhibit the same configuration at the asymmetric carbon atom (C47, C61, C75, and C89, respectively), although X-ray crystallography did not permit

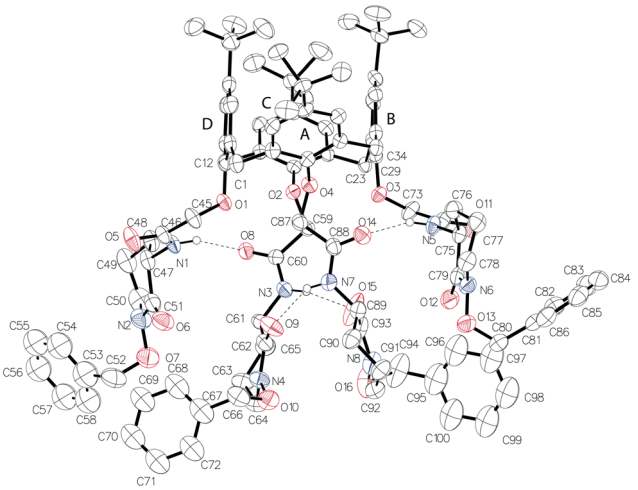

Fig. 3 ORTEP[17] picture of $1Bn_4$ viewed along the direction of rings A and C. All C–H hydrogen atoms have been omitted for clarity. Thermal ellipsoids are drawn at the 50% probability level. Hydrogen bonds are represented by dashed lines.

determining the absolute configuration of $1Bn_4$. However, assuming that the chirality of the amine 7 remains unchanged in the course of amide bond formation, the chirality of the modified calix[4]arene should be (*R*,*R*,*R*,*R*)-$1Bn_4$. Interestingly, intramolecular hydrogen bonds that maintain the calixarene platform in its pinched-cone conformation, can be detected between the amide protons and the carbonyl oxygen atoms belonging to pairs of adjacent strands (Table 1).

Mass spectrometric analyses of $1Bn_4$ and $1H_4$

Both calix[4]arenes were examined by high resolution ESI mass spectrometry, and both showed two manifolds. The most intense massif was the one corresponding to the sodium adduct $[M + Na]^+$ with the most intense line appearing at m/z = 1712.868 for $1Bn_4$ and 1351.685 for $1H_4$, while the other was assigned to the disodium adduct $[M + 2\ Na]^{2+}$ at m/z = 867.929 and 687.337, respectively. In both cases, the experimental monoisotopic distribution patterns perfectly match the calculated ones (Fig. S2–S5, ESI†). In contrast, MALDI-TOF mass spectra evidenced only the signals of $[M + Na]^+$.

NMR characterisation of $1Bn_4$ and $1H_4$

The calix[4]arenes were fully characterized by ^1H and ^{13}C NMR spectroscopy, and the signals were assigned using 2D ^1H–^1H

Table 1 Intramolecular hydrogen bond distances (Å) and angles (°) for $1Bn_4$[a]

N–H···O	*d*(H···O)	*d*(N···O)	<(NH···O)
N1–H1···O8	2.09	2.918(5)	156.4
N3–H3A···O15	1.90	2.747(5)	162.3
N5–H5A···O14	2.07	2.887(5)	153.0
N7–H7···O9	1.96	2.764(5)	151.3

[a] *d*(N–H) = 0.88 Å for all bonds.

COSY and ROESY, ^{13}C–^{1}H HSQC and HMBC techniques (Fig. S6–S18, ESI†). Signal attribution started from *tert*-butyl (H-7) and amide (N–H) protons and the other protons were assigned step by step, using the informations collected from the COSY and ROESY spectra. The signals of **1**Bn_4 are relatively broad in $CDCl_3$, except those of the dangling benzyl protecting groups and the doublet of equatorial H-3 (3e). The signals of **1**H_4 are even broader, pointing to the occurrence of hydrogen bonds involving the hydroxamic acid units. Hence, the spectral resolution was improved by exchanging CD_3OD for $CDCl_3$. In fact, the spectrum of **1**H_4 in CD_3OD is very similar to the one of **1**Bn_4 in $CDCl_3$, except that the axial H-3 (3a) protons show up as the expected doublet, whereas in the case of **1**Bn_4 the signal looks like a very broad singlet. The presence of four equivalent groups of diastereotopic $ArCH_2Ar$ methylenic protons for both **1**Bn_4 and **1**H_4 indicates that the calix[4]arene scaffolds are also in the cone conformation in solution.[20] The fact that the spectra are diagnostic of C_4-symmetric structures confirms that the asymmetric C-12 (labelled C47, C61, C75, and C89 in the ORTEP view of Fig. 3) has the same absolute configuration in each branch (*R*) as in compound **7**. Chemical shift values of homologous protons belonging to both compounds are compared in Table 2. It turned out that the best resolved spectrum of **1**H_4 was obtained after heating the free ligand for 1 h at 60 °C in CD_3OD in the presence of one equivalent of Na^+ (Fig. S19, ESI†), whereas the signal sharpening was less pronounced in the presence of K^+ (Fig. S20, ESI†). These results are in agreement with the recognized ability of *O*-substituted calix[4]arenes appended to –CH_2–C(O)– groups to behave as alkali-cation receptors.[12b,14] The consequences of the central chirality of the C-12 atom of each pendant cyclic hydroxamic acid is better seen in the ^{13}C NMR spectrum of **1**H_4 in CD_3OD, as the diastereotopic C-2 (C-2′) and C-4 (C-4′) aromatic carbon atoms clearly show up as distinct singlets at 135.0 (134.4) and 126.9 (126.5) ppm, respectively (Table 3). By contrast, in the case of **1**Bn_4 ($CDCl_3$) these diastereotopic carbon atoms show degenerate signals at 132.2 and 125.7 ppm, respectively.

Complexation studies

In earlier work we have shown that the cyclic hydroxamic acid 1-hydroxypiperidine-2-one (1,2-PIPOH) was able to form octacoordinated ML_4 complexes with tetravalent metal cations such as Zr^{4+}, Hf^{4+}, Ce^{4+}, Th^{4+}, and U^{4+}.[3g] Typically, $Zr(acac)_4$ or $Hf(acac)_4$ was reacted with four equivalents of 1,2-PIPOH in methanol at room temperature to afford the corresponding neutral complexes $Zr(1,2\text{-PIPO})_4$ and $Hf(1,2\text{-PIPO})_4$ in 57 and 59% yields after crystallization from CH_2Cl_2–heptane 1 : 3 v/v. Single crystal X-ray analysis of these complexes showed that the tetravalent metal cations have a distorted square-antiprismatic geometry of D_2 symmetry, because of the alternate arrangement of the $[O–(N–C)=O]^-$ chelates, two neighbouring ones displaying opposite orientations with respect to the N and C atoms of the six-membered ring. The ^{1}H and ^{13}C NMR spectra of the complexes in $CDCl_3$ evidence sharp signals that are also fully consistent with D_2 symmetry.

Hence, in a first attempt to prepare the zirconium complex of the tetrahydroxamic acid **1**H_4, an equimolar amount of free ligand was reacted directly in a NMR tube with $Zr(acac)_4$ in CD_3OD at room temperature. The ^{1}H NMR spectrum of the crude reaction mixture showed broad signals in the same regions as for the free ligand, but also broad features in the aromatic range around 6.5 and 7.2 ppm, including the characteristic singlet arising from the 4-H protons of uncomplexed **1**H_4 (Fig. S21b, ESI†). Heating the mixture at 55–60 °C for 1.5 h resulted in significant changes in the NMR spectrum, in particular, the disappearance of all the signals corresponding to the free ligand and the concomitant growth of clearly identifiable singlets protruding from broad features in the aromatic region (Fig. S21c, ESI†). The MALDI-TOF mass spectrum of the mixture showed, in addition to the expected signals corresponding to the $[Zr(\mathbf{1}) + Na]^+$ cation, clusters of peaks corresponding to $[Zr_2(\mathbf{1})_2 + Na]^+$ and $[Zr_2(\mathbf{1})_2 + K]^+$.

These latter observations prompted us to run the same reaction (CD_3OD, 60 °C) in the presence of half an equivalent of KCl. As expected, the intensity of the signal corresponding to

Table 2 Selected ^{1}H NMR data for **1**Bn_4 and **1**H_4 in CD_3OD[a]

Compd/H-	3a	3e	4,4′	7	8,8′	12	13,13′	14,14′	17,17′[b]
1Bn_4	4.77	3.30	6.91	1.12	4.73	4.64	1.82/2.02	1.93	4.86/4.91
1H_4	4.72	3.24	6.86	1.10	4.67	4.59	1.94/2.05	2.01	—

[a] δ (ppm) *vs.* TMS. [b] CH_2 protons of the Bn protecting group.

Table 3 Selected ^{13}C NMR data for **1**Bn_4 and **1**H_4[a]

Compd/C-	1	2,2′	3	4,4′	5	6	7	8	9	12
1Bn_4[b]	155.1	132.2	32.7	125.7	145.0	33.9	31.5	74.8	171.2	50.2
1H_4[c]	154.5	135.0, 134.4	33.0	126.9, 126.5	146.5	34.8	31.9	75.4	172.1	51.3

[a] δ (ppm) *vs.* TMS. [b] $CDCl_3$. [c] CD_3OD.

the K^+ adduct at $m/z = 2872.88$ was enhanced in the MALDI-TOF mass spectrum after KCl addition (Fig. 4 and S22, ESI†), while the major signal found by ESI-MS corresponded to the doubly-charged $[Zr_2(\mathbf{1})_2 + 2K]^{2+}$ species (Fig. S24, ESI†). Most interestingly, the ^{1}H NMR spectrum of the reaction mixture revealed also dramatic changes as compared to the one recorded in the absence of K^+ ions (Fig. S25, ESI†), clearly evidencing a strong interaction of the alkali metal with the calixarene zirconium complex in solution rather than a weak ion-pair formation in the gas phase. Very similar features were noted in the ^{1}H NMR spectrum of the corresponding hafnium complex, pointing to related stoichiometries and structures, as expected considering the almost identical ionic radii of octacoordinated Zr^{4+} ($r_i = 0.84$ Å) and Hf^{4+} ($r_i = 0.83$ Å).[21] Due to slightly higher resolution, the latter is reproduced in Fig. 5 together with the signal assignments. In the aromatic region, several doublets are clustered around 7.20 ppm, while four more appear between 6.40 and 6.60 ppm. In the 5.7–3.0 ppm range, several doublets of equal intensities and multiplets with more complex patterns can be recognized. In addition, four predominant singlets scattered between 1.25 and 1.50 ppm on the one hand, and between 0.75 and 1.00 ppm on the other hand, can also be identified in the region of the *tert*-butyl protons (H-7).

An illustrative summary of the various ^{1}H NMR complexation experiments discussed is presented graphically in Fig. S26 (ESI†), in the form of a stacked plot of the spectra obtained after reacting $\mathbf{1}H_4$ with respectively KCl (1 : 1), Hf(acac)$_4$ (1 : 1), and Hf(acac)$_4$ + KCl (1 : 1 : 0.5).

Assuming a $[M_2K(\mathbf{1})_2]^+$ stoichiometry for the complexes, the ^{1}H NMR spectrum of $[Hf_2K(\mathbf{1})_2]^+$ reproduced in Fig. 5 would correspond to a species in which the two Hf(**1**) subunits are equivalent, while the calix[4]arene ligand has lost its C_4 symmetry upon complexation, becoming asymmetric in the complex. As a matter of fact, each of the four legs of the tetrapod $\mathbf{1}^{4-}$ is inequivalent in the complex, which is accounted for hereafter by the use of four different labels (A, C, E, and G). The coordination sphere of each tetravalent metal cation being satisfied with four bidentate hydroxamate subunits, dimer formation can result from the binding of the bridging metal cations by chelates belonging to two different tetrapods, either in the 2 : 2 or the 3 : 1 ratio. A reasonable illustration of the first situation (D_2 symmetric complex) is shown in Fig. 6a, where two binding groups located *trans* to each other at a given metal centre belong to the same calix[4]arene subunit. As a consequence, the chelating subunits of the dimer can be partitioned into two groups of equivalent systems schematized by blue and pink colours in Fig. 6a. Obviously, this arrangement cannot account for the ^{1}H NMR observations. On the contrary, the situation in which three hydroxamate groups are provided by one calix[4]arene and the fourth one by the second molecule of ligand in order to complete the coordination sphere of each metal cation, leads to a C_2-symmetric complex in which all four chelates are in different chemical environments (Fig. 6b).

As shown in Fig. 5 for the hafnium complex, nearly complete assignment of the ^{1}H NMR spectrum could be achieved by a combined analysis of the ^{1}H–^{1}H COSY and ROESY, ^{13}C–^{1}H HSQC and HMBC correlation charts (Fig. S27–S33, ESI†). Thanks to the temperature dependence of certain proton resonances, comparison of the spectra recorded at 300 and 335 K was particularly useful for identifying overlapped signals (Fig. S34, ESI†). The COSY spectrum allowed at first to recognize the eight diastereotopic H-8/H-8′ and H-3a/H-3e proton pairs, the assignment of which being later confirmed by the analysis of the HSQC spectrum. In particular, resonances H-3$_D$e and H-3$_H$e could be differentiated in the 300 K HSQC spectrum of the hafnium complex (Fig. S32, ESI†). Correlations found in the ROESY spectrum (Fig. 7) then allowed identifying the aromatic groups and the methylene bridges separating them on the one hand, and the proton pairs H-8/H-8′ belonging to the methylene functions of the acetamide groups bridging the phenol and the hydroxamate moieties. Observed NOE effects are marked with arrows in Fig. 8. ROESY cross peaks were found between the proton signals H-7(*t*Bu)/H-4, H-7/H-4′, H-4/H-3e, H-4′/H-3e, and,

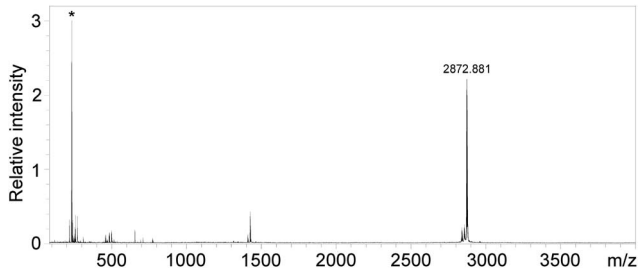

Fig. 4 MALDI-TOF mass spectrum of the reaction product of $\mathbf{1}H_4$, Zr(acac)$_4$ and KCl in 1 : 1 : 0.5 ratio. * marks dithranol (used as matrix).

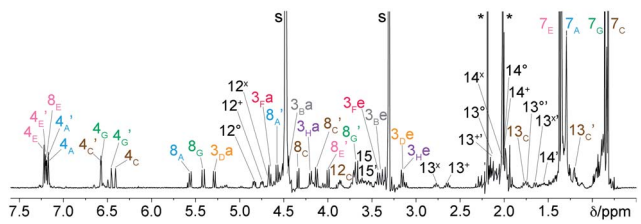

Fig. 5 ^{1}H NMR spectrum (CD_3OD, 335 K) of the $[Hf_2K(\mathbf{1})_2]^+$ complex. The labels s and * denote solvent and acetylacetone, respectively.

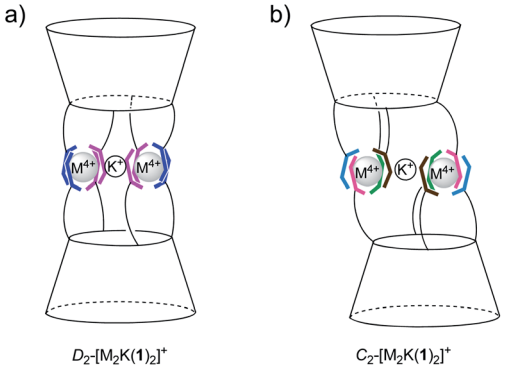

Fig. 6 Two possible structural arrangements of the $[M_2K(\mathbf{1})_2]^+$ dimer. Equivalent chelates are shown in the same colour.

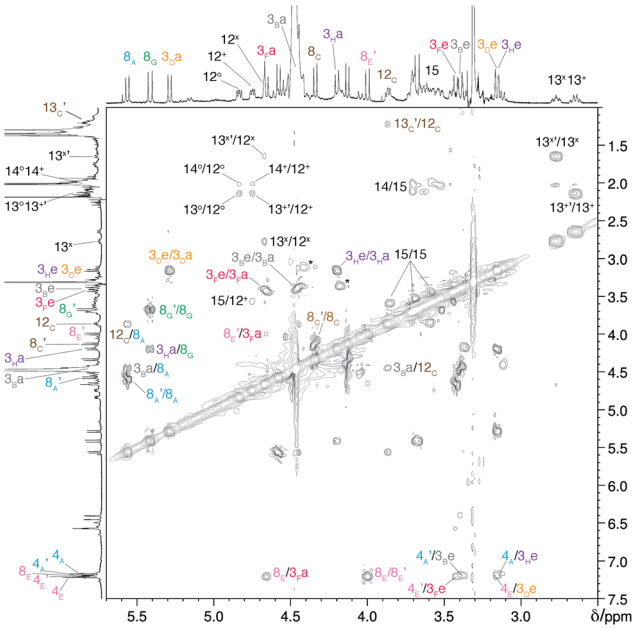

Fig. 7 ROESY NMR spectrum of the $[Hf_2K(\mathbf{1})_2]^+$ complex (CD_3OD, 335 K, mixing time = 200 ms). Starred spots correspond to impurities.

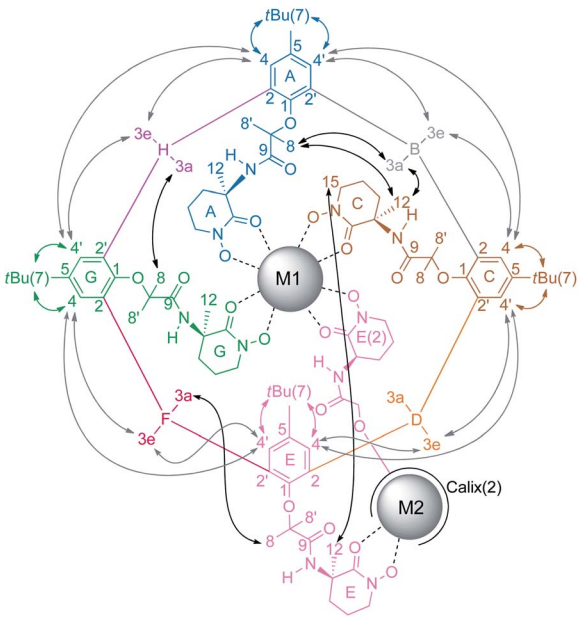

Fig. 8 Map summarizing the NOE cross-correlation peaks found in the ROESY spectrum of the $[M_2K(\mathbf{1})_2]^+$ complexes. The coloured and grey double-ended arrows represent trivial NOE correlations, whereas the black ones point to key correlations for the structural analysis. The drawing is focused on the calix[4]arene ligand that provides three out of the four hydroxamate binding units for chelating the metal centre M1. The fourth group, denoted E(2), bound to M1 but belonging to the second calix[4]arene molecule, labelled calix(2), is also represented together with its symmetry-related component E that binds M2. The potassium cation is omitted.

more specifically, H-3_Ba/H-8_A, H-3_Fa/H-8_E, H-3_Ha/H-8_G, H-4_A/H-4_G′, H-4_G/H-4_E′, H-4_E/H-4_C′, and H-4_C/H-4_A′. The assignments drawn from these correlations were checked for self-consistency by complete analysis of the HMBC spectrum, which also allowed to locate the aryl C-1, C-2/C-2′, C-4/C-4′, and C-5, as well as the amide carbon atoms C-9. In turn, the protons of the bound hydroxamate units were much more difficult to attribute. Four multiplets arising from the H-12 protons attached to the asymmetric carbon centres C-12 and those from the associated pairs of diastereotopic protons H-13/H-13′ could be distinguished. However, resonances corresponding to the proton pairs H-14/H-14′ and H-15/H-15′ could not be assigned without ambiguity, mainly because they are clustered in a very narrow chemical shift range, contrary to the well scattered H-13/H-13′ signals. Unfortunately, it was not possible to correlate H-12 with other identified protons, excepted for H-12_C which gives rise to a through-space correlation with H-3_Ba and H-8_A in the ROESY spectrum. Therefore, the other H-12 and H-13/H-13′ proton signals have been distinguished using a different labelling system (o, +, and ×).

Selected ^{1}H NMR chemical shift values recorded for $[Na(\mathbf{1}H_4)]^+$ and $[Hf_2K(\mathbf{1})_2]^+$ in CD_3OD are compared in Table 4. $[Na(\mathbf{1}H_4)]^+$ was chosen as reference rather than $\mathbf{1}H_4$, because of its increased rigidity.§ Whereas H-4_A/H-4_A′ and H-4_E/H-4_E′ resonate in the same range as H-4/H-4′ for $[Na(\mathbf{1}H_4)]^+$ (7.27 ppm), this is not the case of H-4_C/H-4_C′ and H-4_G/H-4_G′, which give signals around 6.5 ppm. Interestingly, the H-7 proton signals pertaining to $[Hf_2K(\mathbf{1})_2]^+$ are also dispatched in two groups, H-7_A and H-7_E are deshielded by *ca.* 0.17 ppm by comparison with those related to $[Na(\mathbf{1}H_4)]^+$, whereas H-7_C and H-7_G are shielded by *ca.* 0.35 ppm. The three multiplets arising from protons H-12^o, H-12^+, and H-12^x are clustered around 4.75 ppm, which is very close to the chemical shift value found for H-12 in $[Na(\mathbf{1}H_4)]^+$ (4.79 ppm), while Zr complexation induces a nearly 1 ppm (3.84 ppm) shielding of the H-12_C resonance. Whereas the equivalent diastereotopic pairs of protons H-8/H-8′ show up for $[Na(\mathbf{1}H_4)]^+$ as an AB spin system (J_{AB} = 14.1 Hz, $\Delta\nu$ = 55.4 Hz) at 4.56 ppm, only H-8_C/H-8_C′ among the corresponding four pairs of $[Hf_2K(\mathbf{1})_2]^+$ gives such a system at *ca.* 4.24 ppm. The three remaining pairs appear as AX spin systems. H-8_A and H-8_G (~5.5 ppm) are deshielded by nearly 1 ppm upon Zr complexation, H-8_A′ is the only one to remain almost unaffected by the presence of the metal cation ($\Delta\delta$ = −0.031 ppm), while H-8_G′ (3.662 ppm) is noticeably the most shielded signal among the H-8′ ones. Moreover, the ^2J coupling constant for H-8_G/H-8_G′ (16.2 Hz) is significantly higher than those measured for the other sets of H-8/H-8′ resonances (^2J ~ 12–13 Hz). However, the most striking behaviour is that exhibited by proton H-8_E, the resonance of which being deshielded by 2.69 ppm! In $[Na(\mathbf{1}H_4)]^+$, proton H-3a resonates at 4.54 ppm, a value from which the chemical shifts of H-3_Fa, H-3_Ba, and H-3_Ha do not depart significantly, whereas the signal of H-3_Da is shifted downfield by *ca.* 0.74 ppm from that value. By contrast, all of the H-3e protons show up between 3.1 and 3.5 ppm, a chemical-shift range that includes H-3e of $[Na(\mathbf{1}H_4)]^+$. As in $[Na(\mathbf{1}H_4)]^+$, the multiplets assigned to the methylenic hydroxamate protons H-15/H-15′ and the H-14/H-14′ are clustered around *ca.* 3.7 and

§ $[Na(\mathbf{1}H_4)]^+$ was chosen rather than $[K(\mathbf{1}H_4)]^+$ because it showed better resolved signals.

Table 4 Comparison of selected ^{1}H NMR data for $[Na(\mathbf{1}H_4)]^+$ and $[Hf_2K(\mathbf{1})_2]^+$ (δ in ppm) and complexation induced shifts (CIS, $\Delta\delta$) at 300 K (CD_3OD)

Proton/compd	$[Na(\mathbf{1}H_4)]^{+a}$	$[Hf_2(\mathbf{1})_2K]^{+a}$	$\Delta\delta^b$	$[Hf_2(\mathbf{1})_2K]^{+c}$
3a	4.537			
3_Ba		4.445	−0.092	4.461
3_Da		5.275	0.738	5.288
3_Fa		4.634	0.097	4.657
3_Ha		4.157	−0.380	4.198
3e	3.435			
3_Be		3.436	0.001	3.394
3_De		3.163	−0.272	3.156
3_Fe		3.436	0.001	3.424
3_He		3.157	−0.278	3.156
4,4′	7.273			
4_A		7.173	−0.100	7.168
4_C		6.388	−0.885	6.407
4_E		7.226	−0.047	7.222
4_G		6.568	−0.705	6.572
$4_A'$		7.205	−0.068	7.189
$4_C'$		6.573	−0.700	6.577
$4_E'$		7.214	−0.059	7.205
$4_G'$		6.452	−0.821	6.455
7	1.193			
7_A		1.355	0.162	1.353
7_C		0.816	−0.377	0.823
7_E		1.375	0.182	1.374
7_G		0.860	−0.333	0.858
8,8′	4.559			
8_A		5.555	0.996	5.563
8_C		4.328	−0.231	4.388
8_E		7.253	2.694	7.209
8_G		5.407	0.848	5.414
$8_A'$		4.528	−0.031	4.578
$8_C'$		4.142	−0.417	4.130
$8_E'$		3.981	−0.578	3.999
$8_G'$		3.662	−0.897	3.675
12	4.793			
12^o		[d]	—	4.834
12^+		[d]	—	4.748
12^x		4.674	−0.119	—
12_C		3.841	−0.952	3.867

[a] $T = 300$ K. [b] CIS expressed as $\Delta\delta = \delta([Hf_2K(\mathbf{1})_2]^+) - \delta([Na(\mathbf{1}H_4)]^+)$. [c] $T = 335$ K. [d] Hidden.

2.0 ppm, respectively. In contrast, those corresponding to the H-13/H-13′ pairs of protons are scattered between 2.8 and 1.1 ppm, the most deshielded massif being assigned to H-13^x and the most shielded one to H-13_C′, while the largest $\Delta\delta$ value (1.58 ppm) for diastereotopic protons is observed for the H-13^x/$13^{x\prime}$ pair.

The distribution of the proton signals that belong to opposite aromatic systems, *i.e.* H-4_A/H-4_A′ and H-4_E/H-4_E′ (respectively H-7_A and H-7_E) on the one hand, and H-4_C/H-4_C′ and H-4_G/H-4_G′ (respectively H-7_C and H-7_G) on the other hand, with one system shielded by comparison with the other, indicates that the calixarene platforms take up a pinched-cone conformation in $[Hf_2K(\mathbf{1})_2]^+$, as found in the crystal structure of $\mathbf{1}Bn_4$. Interestingly, the most AB-like H-8/H-8′ spin system (the H-8_C/H-8_C′ pair), is also the only one that does not show any H-8/H-3a NOE correlation. The unusual downfield shifts of signals H-8_A, H-8_E, H-8_G, and H-3_Da could be due to deshielding interstrand (for H-8 protons) amide NH···O contacts. These could explain the simultaneous deshielding of H-8_E and H-3_Fa, which also show a NOE contact. There is one additional NOE that was not mentioned so far, namely the one between H-12^+ and a H-15/H-15′ proton. Handling of CPK models suggests that H-12^+ is H-12_E and H-15/H-15′ is H-15_C/H-15_C′, see Fig. 8. All these correlations are consistent with the hypothetical structure of a binuclear complex in which the hydroxamate groups of A, C, and G of a calixarene subunit bind to one M^{4+} cation together with the hydroxamate group E of the other calixarene subunit, providing a coordination environment that should be close to a dodecahedron (Fig. 6b and Scheme 3).

To complement these investigations, diffusion ordered spectroscopy (DOSY) NMR experiments were performed in CD_3OD (Fig. 9). The DOSY chart for the $[Zr_2K(\mathbf{1})_2]^+$ complex revealed the occurrence in solution of a single diffusing species with $D = 301$ μm^2 s^{-1} in addition to methanol-d_4 ($D = 2214$ μm^2 s^{-1}), whereas the diffusion coefficient for the corresponding hafnium complex is 367 μm^2 s^{-1} in the same solvent ($D = 2250$ μm^2 s^{-1}). Taking the value measured for the *in situ* generated monomeric inclusion complex $[K(\mathbf{1}H_4)]^+$ as a reference ($D = 461$ *vs.* 2244 μm^2 s^{-1} for CD_3OD), the diffusion coefficients found for the dimeric zirconium and hafnium complexes are smaller by a factor of 0.65 and 0.80, respectively. It must be noted that a very similar variation was observed between a *meso*-substituted zinc porphyrin precursor bearing four allyl-functionalized polyether chains and the corresponding diporphyrinic cage obtained by ring-closing metathesis.[22]

Taken altogether, ^{1}H NMR observations (spectral analysis and DOSY) as well as mass spectrometry results fully support the formation of a dimer having $[M_2K(\mathbf{1})_2]^+$ formula upon reaction of $M(acac)_4$ with the calix[4]arene tetrapod $\mathbf{1}H_4$

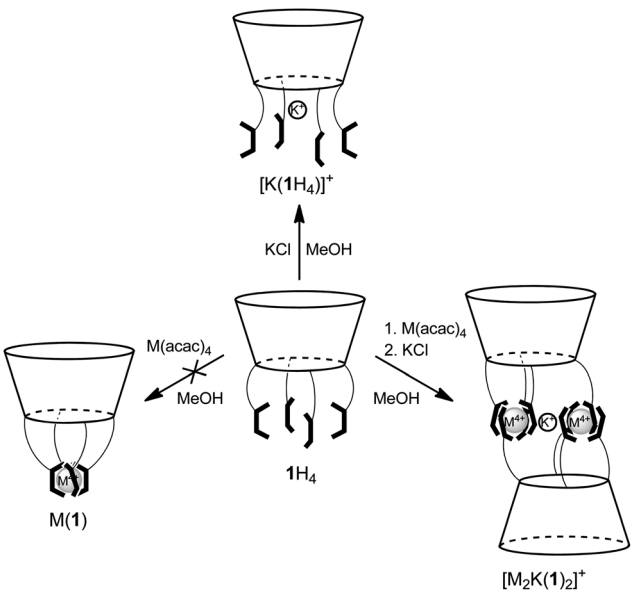

Scheme 3 Summary of the coordination chemistry of $\mathbf{1}H_4$ with $M = Zr^{4+}$ or Hf^{4+}.

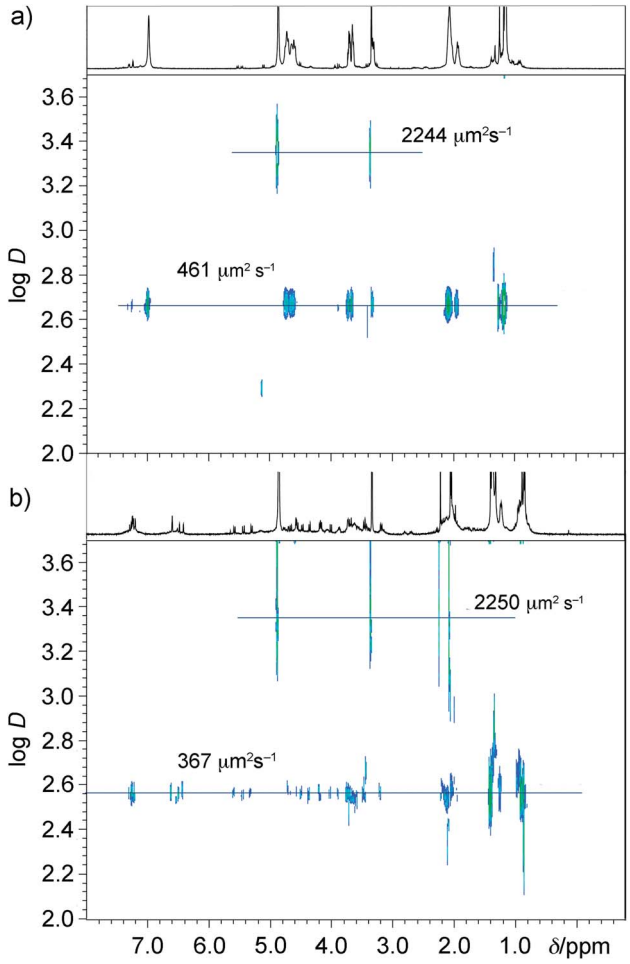

Fig. 9 Comparison of the ^{1}H DOSY NMR spectra (CD_3OD, 300 K) of an equimolar mixture of $\mathbf{1}H_4$ and KCl (a) and of $\mathbf{1}H_4$, $Hf(acac)_4$, and KCl in 1 : 1 : 0.5 molar ratio (b).

featuring 1,2-PIPOH hydroxamic acid binding motifs. As NMR spectroscopy turned out to be the most valuable structural investigation technique, most small scale reactions were run at ~0.01 M concentration levels, which might favour aggregation processes. These are limited to dimerization probably thanks to the preorganization effect of the calix[4]arene platform. However, under more dilute conditions, typically $\sim 10^{-5}$ M, the 2 : 2 species still prevail in solutions as clearly evidenced by HR-ESI-MS analyses. Thus, aggregation of two M(**1**) monomers at higher concentrations, which could be driven by electrostatic or hydrogen-bonding interactions, can be confidently ruled out. Unfortunately, all attempts to crystallize a zirconium or hafnium complex failed, whether an alkali salt was present or not.

For symmetry and stoichiometry reasons, we have arbitrarily located the K^+ cation in the middle of the molecule, where it could interact with the 1,2-$PIPO^-$ oxygen atoms, but the possibility that it could be bound by the eight oxygen atoms of the $-OCH_2C(O)-$ bridges and shuttle rapidly (with respect to the ^{1}H NMR timescale) between these two equivalent sites cannot be ruled out. Some support for this interpretation is provided by the unexpectedly high deshielding effect observed for some signals arising from the H-8 protons, as these might effectively sense the presence of a nearby located K^+ cation. To the best of our knowledge, the $[M_2K(\mathbf{1})_2]^+$ (M = Zr and Hf) complexes represent the first example of a supramolecular assembly involving two M^{4+} cations and two calix[4]arene moieties which share their pendant chelating groups in the coordination sphere of each metal centre, as all the other systems described so far involve μ-bridging ligands, such as the oxide anion[23a] or CH_3OH.[23b]

Our initial design of the calix[4]arene-based hydroxamate tetrapod $\mathbf{1}^{4-}$ relied on the hypothesis that the M^{4+} cation would arrange the four 1,2-$PIPO^-$ binding units in a four-bladed propeller-like fashion, thus imparting a *Λ* or *Δ* helicity to the metal centre (Fig. 2). As each of the chelated hydroxamate incorporates an asymmetric carbon atom (C-12) of *R* configuration, chirality induction could furthermore be anticipated. Accordingly, the bidentate ligands were expected to span four equivalent lateral edges of a twisted square antiprism defined by the oxygen atoms located at the eight vertices, as shown schematically in Fig. 10a. However, the recently solved X-ray crystal structures of $Zr(1,2\text{-PIPO})_4$ and $Hf(1,2\text{-PIPO})_4$ complexes revealed an alternative layout to the C_4-symmetric arrangement, in which the ligands are positioned along opposite edges of the twisted square faces, in pairwise opposite orientations (Fig. 10b).[3g] Clearly, this binding scheme of ideal D_2 symmetry cannot be achieved by a single tetrapod appended with four identical chelating motifs for a 1 : 1 metal-to-ligand species, but in turn can be satisfied by the aforementioned [1 + 3] dimerization process. As a result, a simpler way of encapsulating an octacoordinated cation would be to functionalize the calix[4]arene platform with only two pendant 1,2-PIPOH units, in order to favour a mononuclear species of ML_2 stoichiometry.

Conversely, octacoordinated metals ions larger than Zr^{4+} or Hf^{4+} are expected to favour approaching dodecahedral coordination geometries of limiting ideal D_{2d} symmetry in order to minimize the electrostatic repulsion energy between the oxygen donors.[24] For simple bidentate units, D_{2d} dodecahedral stereochemistries are typically observed when the normalized bite *b* is less than 1.1 [*b* is defined as the O–O/O–M distance ratio or

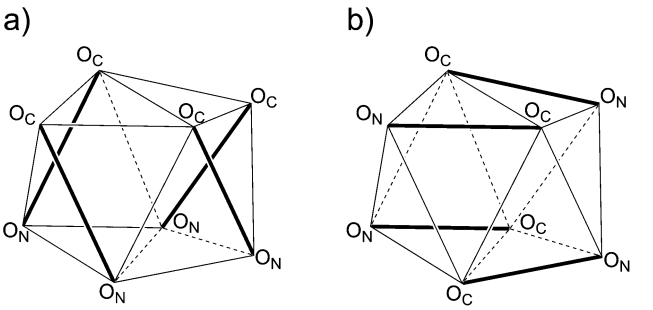

Fig. 10 Slightly distorted square-antiprismatic coordination geometries. (a) Hypothesized arrangement of the bidentate (O_N-O_C) 1,2-$PIPO^-$ ligands required to form a complex of M(**1**) stoichiometry. (b) Experimentally observed arrangement of the hydroxamate groups in the X-ray crystal structure of $Zr(1,2\text{-PIPO})_4$.[3g]

alternatively as a function of the O–M–O bite angle β according to $b = 2\sin(\beta/2)$]. Experimentally, An(1,2-PIPO)$_4$ complexes (An = Th^{4+} or U^{4+}) fulfil that criterion.[3g] Hence, it cannot be excluded that these ions might be tetrachelated by the four dangling hydroxamates of ligand $\mathbf{1}^{4-}$ and afford the sought 1 : 1 inclusion complex. Indeed, provided that the arms are flexible and long enough, the scaffold could properly orient the binding groups around a single metal centre allowing them to span the lateral edges of an approaching dodecahedron, a situation close to the one depicted in Fig. 10a. Work going in that direction is currently under progress.

Conclusions

Developing abiotic metal-uptake agents inspired from natural ligands has proven to be useful in the past, and our approach is nothing but a similar one, using an iron(III) binding motif (1,2-PIPOH) found in a few number of bacterial siderophores. So far essentially ignored by the coordination chemists, cyclic aliphatic hydroxamates, like the six-membered 1,2-PIPO$^-$, represent an interesting alternative to the analogous but aromatic, and thus slightly more acidic, 1,2-HOPO, the binding motif of the single chelate siderophore cepabactin.[25] High-valent transition metals, including lanthanides and actinides, have high coordination numbers (CN), generally equal to or greater than 8. For CN = 8, the most frequently observed coordination polyhedra are the square-antiprism and the trigonal-faced dodecahedron. Accommodation of additional ligands is achieved by capping one or more faces of these polyhedra. It is clear from this study that the design of tetrachelating C_4-symmetric podands for metal ions favouring octacoordination is not a trivial task and requires further tuning for achieving a 1 : 1 metal-to-ligand stoichiometry of the complexed species.

Experimental

General methods and materials

Unless otherwise noted, all chemicals and starting materials were obtained commercially and used without further purification. Toluene and tetrahydrofuran (THF) were dried over sodium/benzophenone, and methanol was dried over magnesium turnings (10% w/v) and iodine (1% w/v). All dried solvents were distilled immediately prior to use. ^{1}H NMR spectra were recorded on a 600 MHz Bruker Avance II spectrometer and referenced internally using the residual protio solvent resonances relative to Me_4Si. Electrospray ionization mass spectra were obtained either on a LTQ Orbitrap XL (HR-MS) or an Amazon SL instrument. MALDI-TOF mass spectra were recorded using an Ultraflex II LRF 2000 instrument and 1,8-dihydroxy-9,10-dihydroanthracen-9-one (dithranol) as matrix. All of these measurements were performed at the "Pôle Chimie Moléculaire", the technological platform for chemical analysis and molecular synthesis (http://www.wpcm.fr) of the Institut de Chimie Moléculaire de l'Université de Bourgogne and Welience™.

X-ray crystallography

X-ray equipment and refinement. Diffraction data were collected on a Nonius Kappa Apex II diffractometer equipped with a nitrogen jet stream low-temperature system (Oxford Cryosystems). The X-ray source was graphite monochromated Mo-Kα radiation ($\lambda = 0.71073$ Å) from a sealed tube. The lattice parameters were obtained by least-squares fit to the optimized setting angles of the entire set of collected reflections. No significant temperature drift was observed during the data collections. Data were reduced by using HKL Denzo and Scalepack software without applying absorption corrections,[26] the missing absorption corrections were partially compensated for by the data scaling procedure in the data reduction. The structure was solved by dual space methods using the SHELXD program.[27] Refinements were carried out by full-matrix least-squares on F^2, using the SHELXL program on the complete set of reflections.[27] Anisotropic thermal parameters were used for non-hydrogen atoms, excepted for disordered molecules of solvent. All H atoms bound on carbon, nitrogen, or oxygen atoms were placed at calculated positions using a riding model with C–H = 0.95 Å (aromatic), 0.98 Å (methyl), 0.99 Å (methylene), N–H = 0.88 Å, and O–H = 0.84 Å, assuming $U_{iso}(H) = 1.2U_{eq.}(CH)$, $U_{iso}(H) = 1.2U_{eq.}(CH_2)$, $U_{iso}(H) = 1.5U_{eq.}(CH_3)$, $U_{iso}(H) = 1.2U_{eq.}(NH)$, and $U_{iso}(H) = 1.5U_{eq.}(OH)$. Similar U_{ij} constraints were applied within the terminal benzyl groups to maintain a reasonable model by using EADP constraints.[27] The geometric parameters in each group were restrained by using AFIX 66 restraints.[27] Heavily-disordered methanol (s.o.f. = 0.75) and water molecules (s.o.f. = 0.25) were refined isotropically.

Crystal data for $\mathbf{1H_4}$. $C_{100}H_{120}N_8O_{16}\cdot 0.75CH_3OH\cdot 0.25\cdot H_2O$, $M = 1718.06$ g mol^{-1}, monoclinic space group $P2_1$ (no. 4), $a = 15.6125(2)$ Å, $b = 18.2100(3)$ Å, $c = 18.3284(3)$ Å, $\beta = 101.79(1)^\circ$, $V = 5100.9(3)$ Å^3, $T = 115$ K, $Z = 2$, μ(Mo-Kα) = 0.076 mm^{-1}, $d_{calc} = 1.119$ g cm^{-3}, 66 668 reflections measured ($8.154 \leq 2\theta \leq 54.934^\circ$), 22 535 unique ($R_{int} = 0.0437$) which were used in all calculations. The final R_1 was 0.0703 [$I > 2\sigma(I)$] and wR_2 was 0.2007 (all data).

Synthesis

Compound 8. 5,11,17,23-Tetra-*tert*-butyl-25,26,27,28-tetracarboxymethoxycalix[4]arene[14] (0.500 g, 0.57 mmol) and thionyl chloride (4.0 mL, 55.14 mmol) were heated in refluxing dry toluene (8 mL) for 4 h. Excess thionyl chloride and the solvent were removed under reduced pressure to afford compound **8** (0.340 g) in 62% yield, which was used without purification in the next step. ^{1}H NMR ($CDCl_3$, 600 MHz, 300 K): δ 1.08 (s, 36H), 3.27 (d, 4H, $^2J = 12.0$ Hz), 4.61 (d, 4H, $^2J = 12.0$ Hz), 5.12 (s, 8H), 6.80 (s, 8H) ppm.

Compound $\mathbf{1Bn_4}$. A solution of $\mathbf{7}\cdot HBr$[13] (0.422, 1.40 mmol), Et_3N (0.152 g, 1.50 mmol, 0.21 mL) in THF (25 mL) was stirred for 1 h and transferred *via* cannula into a stirred solution of the chlorocarbonylmethoxy derivative **8** (0.340 g, 0.35 mmol) in THF (20 mL). The reaction mixture was refluxed for 45 h then diluted with 150 mL of CH_2Cl_2, washed with water (3 × 20 mL), dried over $MgSO_4$, filtered and concentrated on a rotary evaporator to give a yellowish crude product (0.678 g), which was fractionally

crystallized from hot CH_3OH (2 mL) to afford pure compound **1**Bn_4 (0.249 g) in 49% yield. Mp 187.4–188.1 °C. ^{1}H NMR ($CDCl_3$, 600 MHz, 300 K): δ 8.473 (br s, 4H, NH), 7.389 (m, 8H, H-19), 7.295 (m, 12H, H-20, H-21), 6.763 (br d, 8H, ^2J = 12.6 Hz, H-4, H-4′), 4.990 (d, 4H, ^2J = 10.2 Hz, H-17′), 4.933 (br s, 4H, H-3a), 4.861 (hidden, 4H, H-12), 4.852 (d, 8H, ^2J = 10.2 Hz, H-17), 4.803 (br d, 8H, ^2J = 9.6 Hz, H-8), 3.385 (m, 4H, H-15′), 3.273 (br d, 4H, H-15), 3.219 (d, 4H, ^3J = 13.2 Hz, H-3e), 1.89–2.01 (m, 8H, H-13′, H-14, H-14′), 1.710 (br s, 4H, H-13), 1.077 (s, 36H, H-7) ppm. ^{13}C NMR ($CDCl_3$, 150 MHz, 300 K): δ 171.2 (C-9), 167.8 (C-16), 155.1 (C-1), 145.0 (C-5), 135.7 (C-18), 132.2 (C-2), 129.6 (C-19), 128.6 (C-21), 128.5 (C-20), 125.7 (C-4), 75.8 (C-17), 74.8 (C-8), 50.8 (C-15), 50.2 (C-12), 33.9 (C-6), 32.7 (C-3), 31.5 (C-7), 27.9 (C-14), 21.1 (C-13) ppm. HR-MS (ESI) *m*/*z* calcd for $[C_{100}H_{120}N_8O_{16}Na]^+$: 1711.871 (monoisotopic mass), found: 1711.868. Elemental analysis % calcd for $C_{100}H_{120}N_8O_{16}$: C, 71.07; H, 7.16; N, 6.63. Found: C, 70.30; H, 7.20; N, 6.67.

Compound 1H$_4$. A mixture of **1**Bn_4 (0.100 g, 60 μmol) and $Pd(OH)_2$/C (20%, 50 mg) in CH_3OH (8 mL) was stirred under an atmosphere of dihydrogen for 15 min. It was subsequently filtered through a pad of silica (70–200 μm), which was washed with CH_3OH and CH_2Cl_2. The filtrate was evaporated to dryness to afford pure **1**H_4 (0.072 g) in 93% yield. Mp 194.0–195.0 °C. ^{1}H NMR (CD_3OD, 600 MHz, 300 K): δ 8.847 (br s, 4H, NH), 6.855 (br s, 8H, H-4, H-4′), 4.723 (d, 4H, ^2J = 13.2 Hz, H-3a), 4.666 (AB, 8H, J_{AB} = 13.8 Hz, $\Delta\nu$ = 23.2 Hz, H-8,8′), 4.588 (m, 4H, H-12), 3.672 (m, 4H, H-15′), 3.598 (m, 4H, H-15), 3.236 (d, 4H, ^2J = 13.2 Hz, H-3e), 2.05 (m, 12H, H-13′, H-14, H-14′), 1.940 (br m, 4H, H-13), 1.100 (s, 36H, H-7) ppm. ^{13}C NMR (CD_3OD, 150 MHz, 300 K): δ 172.1 (C-9), 167.2 (C-16), 154.5 (C-1), 146.5 (C-5), 135.0 (C-2′), 134.4 (C-2), 126.9 (C-4′), 126.5 (C-4), 75.4 (C-8), 52.3 (C-15), 51.3 (C-12), 34.8 (C-6), 33.0 (C-3), 31.9 (C-7), 28.6 (C-13), 21.8 (C-14) ppm. HR-MS (ESI) *m*/*z* calcd for $[C_{72}H_{96}N_8O_{16}Na]^+$: 1351.684, found: 1351.686; calcd for $[C_{72}H_{96}N_8O_{16}Na_2]^{2+}$: 687.336, found: 687.337. Elemental analysis % calcd for $C_{72}H_{96}N_8O_{16}\cdot 4H_2O$: C, 61.70; H, 7.48; N, 7.99. Found: C, 61.49; H, 7.19; N, 7.78.

Complexation experiments

Reaction of 1H$_4$ with NaCl. **1**H_4 (4.08 mg, 3.07 μmol) was dissolved in CD_3OD (0.7 mL) and the ^{1}H NMR spectrum of the resulting solution recorded. Next, solid NaCl (0.18 mg, 3.08 μmol) was added to the solution of the calix[4]arene **1**H_4 and the reaction mixture heated to 60 °C overnight. Changes in the ^{1}H NMR spectrum were recorded. ^{1}H NMR (CD_3OD, 600 MHz, 300 K): δ 7.273 (s, 8H, H-4, H-4′), 4.793 (dd, 4H, ^3J = 10.2 Hz, ^3J = 5.4 Hz, H-12), 4.559 (AB, 8H, J_{AB} = 14.1 Hz, $\Delta\nu$ = 55.4 Hz, H-8, H-8′), 4.537 (d, 4H, ^2J = 12.6 Hz, H-3a), 3.71–3.63 (m, 8H, H-15, H-15′), 3.435 (d, 4H, ^2J = 12.6 Hz, H-3e), 2.15–2.22 (m, 4H, H-13), 2.00–2.14 (m, 8H, H-14, H-14′), 1.839 (m, 4H, H-13′), 1.193 (s, 36H, H-7) ppm. ^{13}C NMR (CD_3OD, 150 MHz, 300 K): δ 171.6 (C-9), 167.3 (C-16), 152.3 (C-1), 149.4 (C-5), 136.1 (C-2), 127.4 (C-4), 75.8 (C-8), 52.4 (C-15), 51.0 (C-12), 35.2 (C-6), 31.8 (C-7), 31.3 (C-3), 28.8 (C-13), 21.8 (C-14) ppm.

Reaction of 1H$_4$ with KCl. **1**H_4 (5.3 mg, 3.99 μmol) was dissolved in CD_3OD (0.7 mL) and solid KCl (0.30 mg, 4.0 μmol) was subsequently added to the solution of the calix[4]arene. The reaction mixture was heated at 60 °C overnight, after which time the changes in the ^{1}H NMR spectrum were recorded. ^{1}H NMR (CD_3OD, 600 MHz, 300 K): δ 7.02 (s, 8H, H-4, H-4′), 4.64 (d, 8H, ^2J = 12.6 Hz, H-3a, H-12), 4.61 (AB, 8H, J_{AB} = 13.6 Hz, $\Delta\nu$ = 95 Hz, H-8, H-8′), 3.72–3.59 (m, 8H, H-15, H-15′), 2.12–1.96 (m, 12H, H-13, H-14, H-14′), 1.94–1.82 (m, 4H, H-13′), 1.14 (s, 36H, H-7) ppm (H-3e hidden under the solvent signal).

Reaction of complex [K(1H$_4$)]$^+$ with Zr(acac)$_4$ and 1H$_4$. To the previous solution were added 1 equiv. of solid **1**H_4 (5.8 mg, 4.36 μmol) and 2 equiv. of $Zr(acac)_4$ (4.1 mg, 8.34 μmol). The reaction mixture was heated at 60 °C overnight and the ^{1}H NMR spectrum subsequently recorded. ^{1}H NMR (CD_3OD, 600 MHz, 295 K): δ 7.258 (d, 2H, ^2J = 13.8 Hz, H-8$_E$), 7.226 (d, 2H, ^4J = 2.4 Hz, H-4$_E$), 7.215 (d, 2H, ^4J = 3.0 Hz, H-4$_E$′), 7.210 (d, 2H, ^4J = 2.4 Hz, H-4$_A$′), 7.174 (d, 2H, ^4J = 2.4 Hz, H-4$_A$), 6.574 (d, 2H, ^4J = 2.4 Hz, H–4$_C$′), 6.564 (d, 2H, ^4J = 2.4 Hz, H-4$_G$), 6.453 (d, 2H, ^4J = 3.0 Hz, H-4$_G$′), 6.385 (d, 2H, ^4J = 2.4 Hz, H–4$_C$), 5.545 (d, 2H, ^2J = 12.6 Hz, H-8$_A$), 5.412 (d, 2H, ^2J = 16.2 Hz, H-8$_G$), 5.274 (d, 2H, ^2J = 12.6 Hz, H-3$_D$a), 4.850 (hidden, 2H, 12°), 4.758 (dd, 2H, ^3J = 10.2 Hz, ^3J = 6.0 Hz, H-12$^+$), 4.707 (d, 2H, ^3J = 4.2 Hz, H-12^x), 4.628 (d, 2H, ^2J = 13.2 Hz, H-3$_F$a), 4.520 (d, 2H, ^2J = 12.6 Hz, H-8$_A$′), 4.443 (d, 2H, ^2J = 13.2 Hz, H–3$_B$a), 4.336 (d, 2H, ^2J = 12.0 Hz, H-8$_C$), 4.154 (d, 2H, ^2J = 12.6 Hz, H-3$_H$a), 4.142 (d, 2H, ^2J = 12.6 Hz, H-8$_C$′), 3.978 (d, 2H, ^2J = 13.8 Hz, H-8$_E$′), 3.858 (dd, 4H, ^3J = 9.0 Hz, H-12$_C$, H-15, H-15′), 3.75–3.50 (m, 14H, H-15, H-15′), 3.660 (d, 2H, H-8$_G$′), 3.438 (d, 2H, ^2J = 12.0 Hz, H-3$_F$e), 3.387 (d, 2H, ^2J = 13.2 Hz, H-3$_B$e), 3.163 (d, 2H, ^2J = 13.2 Hz, H-3$_D$e), 3.159 (d, 2H, ^2J = 13.8 Hz, H-3$_H$e), 2.745 (m, 2H, H-13^x), 2.679 (m, 2H, H-13$^+$), 2.2–1.9 (several m, 16H, H-13°, H-13$^{+\prime}$, H-14, H-14′), 1.765 (two m, 4H, H-13$_C$, H-13°′), 1.655 (br d, 2H, ^2J = 14.4 Hz, H-13$^{x\prime}$), 1.556 (m, 2H, H-14′), 1.375 (s, 18H, H-7$_E$), 1.354 (s, 18H, H-7$_A$), 1.201 (m, 2H, H-13$_C$′), 0.861 (s, 18H, H-7$_G$), 0.814 (s, 18H, H-7$_C$). MALDI-TOF MS *m*/*z* calcd for $[C_{144}H_{184}KN_{16}O_{32}Zr_2]^+$: 2868.099, found: 2868.910 (monoisotopic mass).

Complexation of 1H$_4$ with Zr(acac)$_4$. $Zr(acac)_4$ (0.75 mg, 1.50 μmol) in CD_3OD (0.5 mL) was added to a solution of **1**H_4 (1.90 mg, 1.43 μmol) in CD_3OD (0.5 mL). The reaction mixture was heated to 55 °C overnight and analyzed by ^{1}H NMR (Fig. S21, ESI†).

One-pot reaction of 1H$_4$ with Zr(acac)$_4$ and KCl. A mixture of **1**H_4 (0.062 g, 47 μmol), $Zr(acac)_4$ (0.023 g, 47 μmol), and KCl (1.8 mg, 23.5 μmol) in CH_3OH (4 mL) was heated to 60 °C. The mixture became homogeneous after 15 min at 60 °C. The solvent was evaporated, leaving a yellowish solid (0.074 g). Analysis by ^{1}H NMR showed that this residue was identical to the material obtained by sequential synthesis.

Reaction of 1H$_4$ with Hf(acac)$_4$ followed by addition of KCl. A solution of $Hf(acac)_4$ (2.61 mg, 4.6 μmol) in CD_3OD (0.2 mL) was added to a suspension of **1**H_4 (6.05 mg, 4.6 μmol) in CD_3OD (0.4 mL). The reaction mixture became immediately clear. The ^{1}H NMR spectrum was run at 333 K to prevent precipitation. Next, KCl (0.76 mg, 10.2 μmol) was added into the NMR tube and the reaction mixture heated at 65 °C overnight. ^{1}H NMR (CD_3OD, 600 MHz, 300 K; signals marked with an * correspond to the spectrum recorded at 335 K): δ 7.253 (d, 2H, ^2J = 13.8 Hz, H-8$_E$), 7.226 (d, 2H, ^4J = 2.4 Hz, H-4$_E$), 7.214 (d, 2H, ^4J = 2.4 Hz, H-4$_E$′), 7.205 (d, 2H, ^4J = 2.4 Hz, H-4$_A$′), 7.173 (d, 2H, ^4J = 2.4 Hz, H-4$_A$),

6.573 (d, 2H, $^4J = 3.0$ Hz, H-4$_C$′), 6.568 (d, 2H, $^4J = 2.4$ Hz, H-4$_G$), 6.452 (d, 2H, $^4J = 2.4$ Hz, H-4$_G$′), 6.388 (d, 2H, $^4J = 1.8$ Hz, H-4$_C$), 5.555 (d, 2H, $^2J = 12.6$ Hz, H-8$_A$), 5.407 (d, 2H, $^2J = 16.2$ Hz, H-8$_G$), 5.275 (d, 2H, $^2J = 12.0$ Hz, H-3$_D$a), *4.834 (dd, 2H, $^3J = 10.8$ Hz, $^3J = 10.8$ Hz, H-12°), *4.748 (d, 2H, $^3J = 10.2$ Hz, $^3J = 6.0$ Hz, H-12$^+$), 4.674 (d, 2H, $^3J = 3.0$ Hz, H-12^x), 4.634 (d, 2H, $^2J = 13.2$ Hz, H-3$_F$a), 4.528 (d, 2H, $^2J = 12.6$ Hz, H-8$_A$′), 4.445 (d, 2H, $^2J = 13.2$ Hz, H-3$_B$a), 4.328 (d, 2H, $^2J = 12.6$ Hz, H-8$_C$), 4.157 (d, 2H, $^2J = 13.2$ Hz, H-3$_H$a), 4.142 (d, 2H, $^2J = 12.0$ Hz, H-8$_C$′), 3.981 (d, 2H, $^2J = 13.8$ Hz, H-8$_E$′), 3.841 (br dd, 4H, H-12$_C$, H-15), 3.75–3.50 (m, 14H, H-15, H-15′), 3.662 (d, 2H, $^2J = 16.2$ Hz, H-8$_G$′), 3.436 (d, 4H, $^2J = 13.8$ Hz, H-3$_B$e, H-3$_F$e), 3.163 (d, 2H, $^2J = 12.6$ Hz, H-3$_D$e), 3.157 (d, 2H, $^2J = 13.2$ Hz, H-3$_H$e), 2.780 (tt, 2H, $^2J = 13.8$ Hz, H-13^x), 2.676 (br q, 2H, H-13$^+$), 2.137 (hidden, 4H, H-13°, H-13$^{+\prime}$), 2.048 (hidden, 2H, H-14^x), 2.010 (hidden, 2H, H-14°), 1.993 (hidden, 2H, H-14$^+$), 2.15–1.85 (m, 8H, H-14, H-14′), 1.788 (br AB, 2H, H-13$_C$), 1.735 (br AB, 2H, H-13°′), 1.649 (br d, 2H, $^2J = 14.4$ Hz, H-13$^{x\prime}$), 1.546 (m, 2H, H-14′), 1.375 (s, 18H, H-7$_E$), 1.355 (s, 18H, H-7$_A$), 1.200 (m, 2H, H-13$_C$′), 0.860 (s, 18H, H-7$_G$), 0.816 (s, 18H, H-7$_C$). MALDI-TOF MS *m*/*z* calcd for $[C_{144}H_{184}KN_{16}O_{32}Hf_2]^+$: 3047.212 (average mass), found: 3047.194 (peak of maximum intensity).

Reaction of 1H$_4$ with KCl followed by addition of Hf(acac)$_4$. A mixture of **1**H$_4$ (64.8 mg, 48.7 μmol) and KCl (1.82 mg, 24.4 μmol) in CH_3OH (20 mL) was heated at reflux for 4 h. Next Hf(acac)$_4$ (28 mg, 48.7 μmol) in CH_3OH (5 mL) was added *via* cannula to the reaction mixture, which was further heated at reflux for 18 h. The mixture became homogeneous after 15 min at 60 °C. The solvent was evaporated, leaving a brown solid (90 mg). Analysis by ^{1}H NMR and MALDI-TOF MS showed that this residue was identical to the material obtained in the previous experiment.

Acknowledgements

This work was supported by the Centre National de la Recherche Scientifique (CNRS), the Conseil Régional de Bourgogne (program PARI IME SMT8), and the Groupement National de Recherche GNR PARIS. P.J. thanks the CNRS and the Conseil Régional de Bourgogne for a PhD fellowship (2009-9201AAO037S03746).

Notes and references

1 A. Lisovskii and M. S. Eisen, *Top. Organomet. Chem.*, 2005, **10**, 63.

2 (*a*) I. Verel, G. W. M. Visser, R. Boellaard, M. Stigter-van Walsum, G. B. Snow and G. A. M. S. van Dongen, *J. Nucl. Med.*, 2003, **44**, 1271; (*b*) T. J. Wadas, E. H. Wong, G. R. Weisman and C. J. Anderson, *Chem. Rev.*, 2010, **110**, 2858; (*c*) L. R. Perk, M. J. W. D. Vosjan, G. W. M. Visser, M. Budde, P. Jurek, G. E. Kiefer and G. A. M. S. van Dongen, *Eur. J. Nucl. Med. Mol. Imaging*, 2010, **37**, 250; (*d*) Y. Zhang, H. Hong and W. Cai, *Curr. Radiopharm.*, 2011, **4**, 131; (*e*) T. K. Nayak, K. Garmestani, D. E. Milenic and M. W. Brechbiel, *J. Nucl. Med.*, 2012, **53**, 113; (*f*) M. A. Deri, B. M. Zeglis, L. C. Francesconi and J. S. Lewis, *Nucl. Med. Bio.*, 2013, **40**, 3; (*g*) G. Fischer, U. Seibold, R. Schirrmacher, B. Wängler and C. Wängler, *Molecules*, 2013, **18**, 6469; (*h*) E. W. Price and C. Orvig, *Chem. Soc. Rev.*, 2014, **43**, 260.

3 (*a*) K. F. Fouche, H. J. Le Roux and F. Phillips, *J. Inorg. Nucl. Chem.*, 1970, **32**, 1949; (*b*) K. Bhatt and Y. K. Agrawal, *Synth. Inorg. Met.-Org. Chem.*, 1972, **2**, 175; (*c*) Y. K. Agrawal and J. P. Shukla, *J. Indian Chem. Soc.*, 1974, **51**, 373; (*d*) M. Pal and R. N. Kapoor, *Indian J. Chem.*, 1980, **19A**, 912; (*e*) T. Moav, A. Hatzor, H. Cohen, J. Libman, I. Rubinstein and A. Shanzer, *Chem.–Eur. J.*, 1998, **4**, 502; (*f*) F. Guérard, Y.-S. Lee, R. Tripier, L. P. Szajek, J. R. Deschamps and M. W. Brechbiel, *Chem. Commun.*, 2013, **49**, 1002; (*g*) P. Jewula, J.-C. Berthet, J.-C. Chambron, P. Thuéry, Y. Rousselin and M. Meyer, manuscript in preparation.

4 P. E. Riley, K. Abu-Dari and K. N. Raymond, *Inorg. Chem.*, 1983, **22**, 3940.

5 G. J.-P. Deblonde, M. Sturzbecher-Hoehne and R. J. Abergel, *Inorg. Chem.*, 2013, **52**, 8805.

6 (*a*) J. Xu, P. W. Durbin, B. Kullgren, S. N. Ebbe, L. C. Uhlir and K. N. Raymond, *J. Med. Chem.*, 2002, **45**, 3963; (*b*) R. J. Abergel, P. W. Durbin, B. Kullgren, S. N. Ebbe, J. Xu, P. Y. Chang, D. Y. Bunin, E. A. Blakely, K. A. Bjornstad, C. J. Rosen, D. K. Shuh and K. N. Raymond, *Health Phys.*, 2010, **99**, 401.

7 G. J. Sharman, D. H. Williams, D. F. Ewing and C. Ratledge, *Chem. Biol.*, 1995, **2**, 553.

8 S. Kodani, M. Ohnishi-Kameyama, M. Yoshida and K. Ochi, *Eur. J. Org. Chem.*, 2011, 3191.

9 S. Dhungana, M. J. Miller, L. Dong, C. Ratledge and A. L. Crumbliss, *J. Am. Chem. Soc.*, 2003, **125**, 7654.

10 (*a*) M. Lee, S.-J. Lee and L.-H. Jiang, *J. Am. Chem. Soc.*, 2004, **126**, 12724; (*b*) F. Corbellini, A. Mulder, A. Sartori, M. J. W. Ludden, A. Casnati, R. Ungaro, J. Huskens, M. Crego-Calama and D. N. Reinhoudt, *J. Am. Chem. Soc.*, 2004, **126**, 17050; (*c*) H. Huang, D. M. Li, W. Wang, Y.-C. Chen, K. Khan, S. Song and Y.-S. Zheng, *Org. Biomol. Chem.*, 2012, **10**, 729.

11 (*a*) R. Ludwig, H. Matsumoto, M. Takeshita, K. Ueda and S. Shinkai, *Supramol. Chem.*, 1995, **4**, 319; (*b*) L. Bennouna, J. Vicens and Z. Asfari, *J. Inclusion Phenom. Macrocyclic Chem.*, 2001, **40**, 96; (*c*) U. V. Trivedi, S. K. Menon and Y. K. Agrawal, *React. Funct. Polym.*, 2002, **50**, 205; (*d*) B. Boulet, C. Bouvier-Capely, C. Cossonnet and G. Cote, *Solvent Extr. Ion Exch.*, 2006, **24**, 319; (*e*) L. Poriel, B. Boulet, C. Cossonnet and C. Bouvier-Capely, *Radiat. Prot. Dosim.*, 2007, **127**, 273; (*f*) B. Boulet, C. Bouvier-Capely, G. Cote, L. Poriel and C. Cossonnet, *J. Alloys Compd.*, 2007, **444–445**, 526; (*g*) A. Leydier, D. Lecerclé, S. Pellet-Rostaing, A. Favre-Réguillon, F. Taran and M. Lemaire, *Tetrahedron*, 2008, **64**, 11319.

12 (*a*) T. Nagasaki, S. Shinkai and T. Matsuda, *J. Chem. Soc., Perkin Trans. 1*, 1990, 2617; (*b*) T. Nagasaki and S. Shinkai, *J. Chem. Soc., Perkin Trans. 2*, 1991, 1063; (*c*) L. Dasaradhi, P. C. Stark, V. J. Huber, P. H. Smith, G. D. Jarvinen and A. S. Gopalan, *J. Chem. Soc., Perkin Trans. 2*, 1997, 1187; (*d*) T. N. Lambert, L. Dasaradhi, V. J. Huber and A. S. Gopalan, *J. Org. Chem.*, 1999, **64**, 6097.

13 L. Dong and M. J. Miller, *J. Org. Chem.*, 2002, **67**, 4759.
14 F. Arnaud-Neu, G. Barrett, S. Cremin, M. Deasy, G. Ferguson, S. J. Harris, A. J. Lough, L. Guerra, M. A. McKervey, M. J. Schwing-Weill and P. Schwinte, *J. Chem. Soc., Perkin Trans. 2*, 1992, 1119.
15 Y.-M. Lin and M. J. Miller, *J. Org. Chem.*, 1999, **64**, 7451.
16 M. R. Johnson, *US Pat.* Appl., 2006 004 0954, 2006.
17 L. J. Farrugia, *J. Appl. Crystallogr.*, 1997, **30**, 565.
18 (*a*) M. A. McKervey, E. M. Seward, G. Ferguson, B. Ruhl and S. J. Harris, *J. Chem. Soc., Chem. Commun.*, 1985, 388; (*b*) G. Calestani, F. Ugozzoli, A. Arduini, E. Ghidini and R. Ungaro, *J. Chem. Soc., Chem. Commun.*, 1987, 344.
19 D. Cremer and J. A. Pople, *J. Am. Chem. Soc.*, 1975, **97**, 1354.
20 J. Scheerder, R. H. Vreekamp, J. F. J. Engbersen, W. Verboom, J. P. M. van Duynhoven and D. N. Reinhoudt, *J. Org. Chem.*, 1996, **61**, 3476.
21 R. D. Shannon, *Acta Crystallogr., Sect. A: Cryst. Phys., Diffr., Theor. Gen. Crystallogr.*, 1976, **32**, 751.
22 J. Taesch, V. Heitz, F. Topić and K. Rissanen, *Chem. Commun.*, 2012, **48**, 5118.
23 (*a*) A. Caselli, L. Giannini, E. Solari, C. Floriani, N. Re, A. Chiesi-Villa and C. Rizzoli, *Organometallics*, 1997, **16**, 5457; (*b*) D.-Q. Yuan, W.-X. Zhu, M.-Q. Xu and Q.-L. Guo, *J. Coord. Chem.*, 2004, **57**, 1243.
24 D. L. Kepert, in *Inorganic Stereochemistry*, Springer Verlag, Heidelberg, 1982.
25 J. M. Meyer, D. Hohnadel and F. Hallé, *J. Gen. Microbiol.*, 1989, **135**, 1479.
26 Z. Otwinowski and W. Minor, *Methods Enzymol.*, 1997, **276**, 307.
27 G. Sheldrick, *Acta Crystallogr., Sect. A: Found. Crystallogr.*, 2008, **64**, 112.

